Article

Research on the Influence of Compression and Offset of Cushion Blocks on the Axial Strength of Transformers

Lu Sun [1,*], **Shuguo Gao** [1], **Tianran Li** [1], **Jiaxin Yao** [2], **Ping Wang** [2] **and Jianhao Zhu** [2]

[1] Hebei Electric Power Research Institute, Shijiazhuang 050021, China; dyy_gaosg@he.sgcc.com.cn (S.G.); dyy_tiany1@he.sgcc.com.cn (T.L.)

[2] Hebei Provincial Key Laboratory of Power Transmission Equipment Security Defense, North China Electric Power University, Baoding 071003, China; 220222213029@ncepu.edu.cn (J.Y.); 51351571@ncepu.edu.cn (P.W.); 220222213199@ncepu.edu.cn (J.Z.)

* Correspondence: dyy_sunl@he.sgcc.com.cn; Tel.: +86-177-6439-1594

Abstract: The instability of the winding-cushion structure is one of the primary causes of transformer failures. Insulation cushion compression and offset are the predominant forms leading to structural instability. Therefore, this paper, using the SFSZ7-31500/110 transformer as an example, first derives the theoretical formula for mechanical stress calculation. It clarifies the key influencing parameters of the winding-cushion block structure on the axial bending stress of the winding. Subsequently, an electromagnetic force finite element calculation model is established to obtain the axial force distribution in the winding and the distribution of unbalanced displacement during short-circuit processes. Based on the force and offset distribution, a specific cushion block compression and offset test platform is constructed. By setting different cushion block variables, the effects of cushion block unbalanced height and cushion block offset on the winding's bending elastic modulus are determined. Finally, a simulation model for stress calculation of the winding-cushion block structure is established, revealing the influence pattern of cushion block compression and offset instability on the axial strength of the winding. The results of this study indicate that the greater the uneven cushion block height, the lower the axial strength of the winding. Under the same cushion block offset angle, winding structures with non-uniform cushion block offsets exhibit the worst axial stability. When the offset angles are $30°$, $45°$, and $60°$, the maximum axial bending stress of the winding increases by 1.73%, 3.46%, and 7.82%, respectively. Increasing the offset angle exacerbates the decrease in the axial strength of the winding up to a certain extent. The findings in this study have significant implications for enhancing a transformer's short-circuit resistance.

Keywords: power transformers; short-circuit impacts; winding strength; cushion blocks; axial bending stress

1. Introduction

Power transformers are essential electrical equipment in the electrical grid that are responsible for critical functions such as energy transmission, flexible allocation, and voltage transformation within the entire power system [1,2]. Consequently, the operational status of transformers directly affects the safety and stability of both local and overall power systems.

During short-circuit incidents, the short-circuit forces acting on transformers can cause insulation and structural component damage, resulting in significant winding deformation and wire breakage [3]. Copper, the most common material used for making transformer windings, is a typical elastoplastic material, while cushion blocks possess a stiffness that gradually hardens [4]. The ability of transformers to withstand short circuits is almost unaffected by minor deformations in windings. However, the cumulative effect of subtle plastic deformations caused by multiple short-circuit impacts can lead to irreversible changes in the mechanical characteristics of windings, resulting in a reduced capacity to

withstand short circuits [5–7]. Under the axial short-circuit electromagnetic force, windings generate axial vibrations, leading to resonance phenomena, collisions, separation between cushion blocks and coil disks, and this ultimately causes winding looseness, distortion, and even collapse [8,9]. Therefore, the study of improving transformer windings, cushion block performance, or structures to enhance their short-circuit withstand capability is of significant importance in engineering.

Numerous scholars have conducted research on the short-circuit strength of transformers. References [10–12] established a mass-spring model that includes cushion blocks, coil disks, pressure plates, and iron cores. Since coil disks experience non-uniform forces on the radial surface, the model divided a coil disk into two mass units and connected them with axial bending springs. Reference [13] researched how increasing the radial width of windings, the number of bracing ribs, and the size of winding subwires can enhance winding strength based on a specific transformer short-circuit test and calculation results. Reference [14] developed a coupled three-dimensional model considering electric, magnetic, and structural fields to investigate the influence of factors such as the insulation paper wrapped around the wire, the tightness of insulation paper tubes, and the Young's modulus on winding strength. Reference [15] studied the distribution of axial forces in windings during transformer short circuits through simulation. Reference [16] proposed a transformer winding deformation online detection method based on VFTO and validated its effectiveness. Reference [17] established a nonlinear vibration model considering axial vibration of windings that deduced and calculated the winding compression force, cushion block and pressure plate compression force, and the axial bending stress of the wires. Reference [18] investigated the impact of cushion blocks on the axial winding strength and of bracing ribs on the radial winding strength, with specific consideration of factors such as the number and width of cushion blocks. References [19,20] indicated that, over the transformer's lifespan, cushion blocks were immersed in dielectric fluid and exposed to high temperatures, thermal aging, and chemical reactions, resulting in the degradation of their dielectric and mechanical properties and weakening the transformer short-circuit resistance. In references [21,22], a two-dimensional simulation was established and the leakage flux and stress distribution of high- and low-voltage winding were analyzed; short-circuit tests were carried out and it was pointed out that the electromagnetic force generated by the fault current might lead to instability in and the collapse of the winding. An improved radial buckling analysis method was proposed to study the radial stability of the inner winding. In reference [23], a winding and supporting spacers structure model is established under short-circuit conditions, and the influence of the flexibility of the spacers on the critical stress of the inner winding is analyzed through case studies.

Based on an analysis of the existing literature, it can be observed that the cushion blocks, as one of the main support structures of the windings, are less studied in terms of their influencing factors such as different unbalanced heights, offset angles, and offset structures. However, in practical operation, when a transformer experiences a short circuit, the cushions are very prone to compression or loosening, resulting in offset under the impact of short-circuit forces. This ultimately leads to the tilting of the winding, i.e., axial instability. Therefore, studying the impact of cushion compression and offset on the axial strength of windings is of significant importance. Therefore, this paper establishes a calculation model for the mechanical stress of windings, considering two types of cushion block fault modes that can cause axial instability in the windings. The maximum axial bending stress calculation formula was revised. A platform for cushion block compression and offset testing was set up. The experiment analyzed the impact of cushion block unbalanced height and offset on the elastic modulus of the wire. Modeling and simulation were conducted using the SFSZ7-31500/110 transformer as a prototype, and the simulation results were combined to validate the effectiveness of the experiments. Following the research results of this paper, the short-circuit force under the condition of pad shrinkage and offset can be considered in order to calculate the short-circuit force, to simulate more realistic

transformer multiple short-circuit impact conditions, and to calculate the short-circuit force more accurately and in greater detail.

2. Study of the Axial Strength of Windings under Short-Circuit Force

In order to study the axial mechanical stress on windings under short-circuit forces, a mechanical stress calculation model for windings was established, as shown in Figure 1.
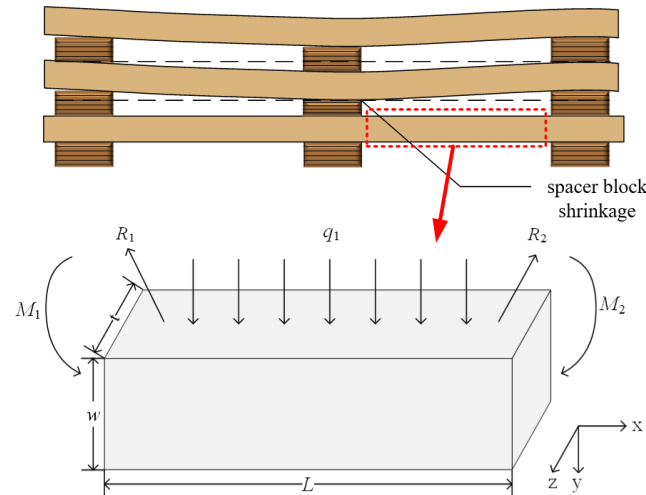

Figure 1. Winding mechanical stress calculation model.

For transformer windings, the axial electromagnetic forces generated by radial leakage magnetic fields cause axial bending deformations in the windings between two sets of cushion blocks. It is considered that the windings and the two sets of cushion blocks constitute a fixed pivot beam structure at both ends [24]. The axial force load on the winding is uniformly distributed. In Figure 1, q_1 represents the force per unit length acting downward along the winding, while R_1 and R_2 are the support reactions at both ends. M_1 and M_2 denote the bending moments, w stands for the height of the winding, and L represents the length of the winding.

To determine the value of the bending stress, we must first derive the force per unit length q_{st} acting on the wires between the two sets of cushion blocks:

$$q_{st} = \frac{F_Y}{N_s \pi D} \tag{1}$$

where N_s denotes the number of strands of the winding, D denotes the average diameter of the winding, and F_Y denotes the maximum axial force applied to the wire cake.

There are six unknown quantities in the problem, two vertical forces, two horizontal forces, and two bending moments, but only three static equilibrium equations are presented, making it a hyperstatic problem. The two horizontal forces in opposite directions are of equal magnitude, exerting mutual tensile forces on each other. Due to the small magnitude of these forces, they can be disregarded [24]. The two vertical forces are of equal magnitude and act downward in the same direction. Therefore, the support reactions happen at both ends, $R_1 = R_2 = q_1 L/2$, where q_1 is the force per unit length acting downward along the beam. Given that this structure is subjected to uniformly distributed axial force loads, q_1 is equal to q_{st}.

The moment of inertia about the z-axis can be expressed as follows:

$$I_z = \frac{tw^3}{12} \tag{2}$$

where t denotes the radial width of the winding.

Cushion block constraints can be regarded as fixed-end constraints. Because the force of the winding is symmetrical and the constraint form at both ends is the same, the bending moment constrained by the winding is equal, that is, M_1 is equal to M_2. The total bending moment at position x can be expressed as follows:

$$M(x) = \frac{q_1 L x}{2} - \frac{q_1 x^2}{2} - M_1 \qquad (3)$$

The deflection curve equation of the beam should be calculated firstly to obtain the bending moment M_1:

$$\frac{d^2 y}{dx^2} = -\frac{M(x)}{E I_z} \qquad (4)$$

where E is the elastic modulus of the beam.

Substituting (3) into (4), (4) can then be re-written as follows:

$$\frac{d^2 y}{dx^2} = -\frac{1}{E I_z} \left(M_1 - \frac{q_1 L x}{2} + \frac{q_1 x^2}{2} \right) \qquad (5)$$

Integrating (5) once gives the following:

$$\frac{dy}{dx} = \frac{1}{E I_z} \left(M_1 x - \frac{q_1 L x^2}{2} + \frac{q_1 x^3}{2} \right) + C \qquad (6)$$

where C is the integration constant. Since we are investigating a beam structure with fixed supports, it follows that $dy/dx = 0$ at $x = 0$ and $x = L$. Substituting this into (6) yields the integration constant $C = 0$, and (7):

$$M_1 = \frac{q_1 L^2}{12} \qquad (7)$$

Then, (6) can be simplified as follows:

$$\frac{dy}{dx} = \frac{q_1}{E I_z} \left(\frac{L^2 x}{12} - \frac{L x^2}{4} + \frac{x^3}{6} \right) \qquad (8)$$

Integrating (8) again, the integration constant is zero since $y = 0$ at $x = 0$ and $x = 1$, giving the following:

$$y = \frac{q_1}{E I_z} \left(\frac{L^2 x^2}{24} - \frac{L x^3}{12} + \frac{x^4}{24} \right) = \frac{q_1 x^2 (L - x)}{24 E I_z} \qquad (9)$$

The bending moment at position x is obtained by substituting (7) into (3):

$$M(x) = \frac{q_1}{2} \left[x(L - x) - \frac{L^2}{6} \right] \qquad (10)$$

The axial bending stress of the beam is defined as follows:

$$\sigma_x = \frac{M y}{I_z} \qquad (11)$$

where y denotes the length measured downward from the centroid of the beam's cross-section.

From (10), the maximum value $M_{max} = q_1 L^2 / 24$ is obtained when $x = L/2$; the minimum value $M_{min} = -q_1 L^2 / 12$ is obtained when $x = 0$ and $x = L$. As M_{min} has the larger absolute value, $M = -q_1 L^2 / 12$ is chosen. For a given x, when $y = \pm w/2$, σ_x obtains its maximum or

minimum value. Thus, choosing $y = -w/2$, and substituting M, y, and (2) into (11) yields the following:

$$\sigma_{x.max} = \frac{q_1 L^2}{2tw^2} \tag{12}$$

Equation (12) gives the formula for calculating the maximum axial bending stress, and for the parameter of the distance L between two blocks, it is considered that the failure modes that lead to axial instability of the winding include the following: wire inclination, the overlapping of turns, block compression faults under axial forces, and block offset under the interaction of axial and radial forces [25,26]. Both block-related faults lead to axial instability in the winding, where block compression faults affect the block unbalanced height Δl and block offset faults directly affect the block offset angle θ.

Based on this, the radial-adjacent block unbalanced height Δl and block offset angle θ are introduced to modify the distance L between two blocks. The calculation formula for L is as follows:

$$L = \sqrt{\left(\frac{\pi D}{Z} + \frac{t \tan\theta}{2}\right)^2 + \Delta l^2} - W \tag{13}$$

where Z denotes the number of block groups in the radial direction, and W denotes the width of the block. The principle of the revised formula is illustrated in Figure 2.
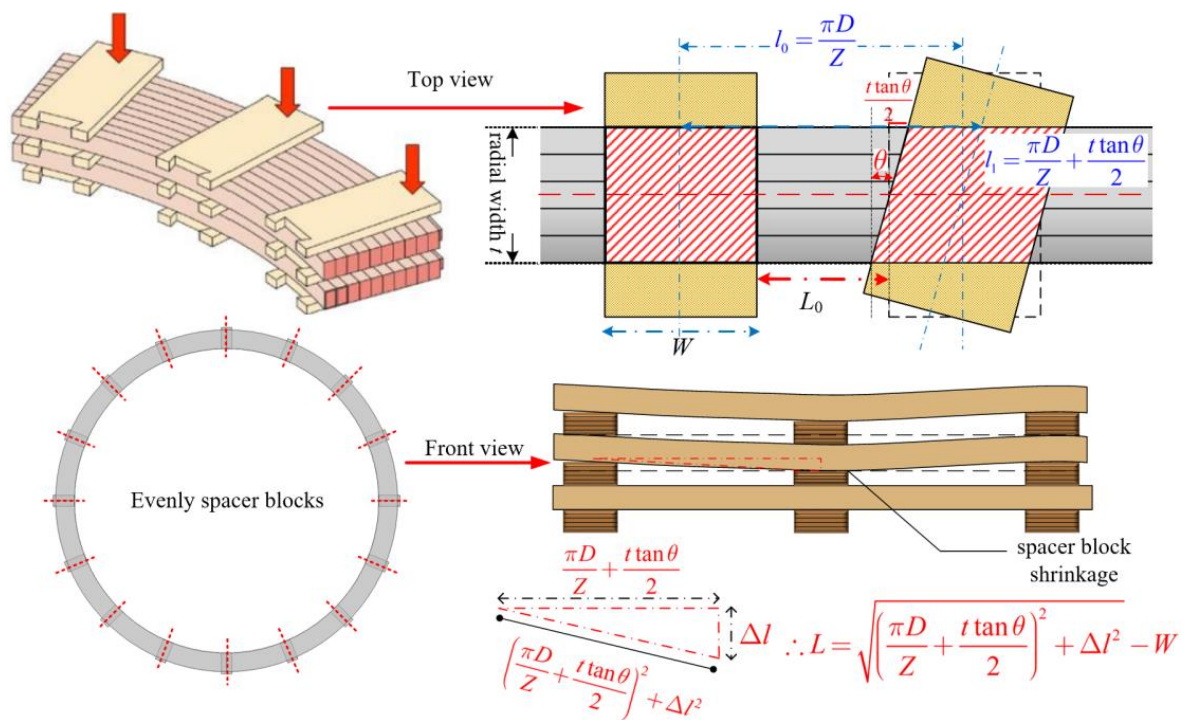

Figure 2. Formula revision illustration diagram.

Substituting (1) and (13) into (12), the maximum axial bending stress between two blocks can be re-expressed as follows:

$$\sigma_{max.axial} = \frac{F_Y}{2NC_s \pi D t w^2} \left(\sqrt{\left(\frac{\pi D}{Z} + \frac{t \tan\theta}{2}\right)^2 + \Delta l^2} - W\right)^2 \tag{14}$$

Following the national standard GB1094.5 [27], the axial bending stress is evaluated and the allowable value standard is less than or equal to 0.9 $R_{p0.2}$.

As indicated by the formula for axial bending stress, it is evident that cushion blocks have a significant impact on the axial strength of transformer windings. Among the influencing factors, the key ones are cushion block unbalanced height and cushion block

offset. Therefore, subsequent analysis primarily focuses on the influence of different cushion block unbalanced heights and different cushion block offsets on the axial strength of windings.

3. Cushion Compression and Offset Test Based on Short-Circuit Force Simulation

In this section, theoretical derivations for electromagnetic force calculations were carried out. A finite element simulation model for transformer electromagnetic forces was constructed. Through simulation, the distribution of axial electromagnetic forces acting on the windings was obtained. Based on this data, the maximum cushion block unbalanced height was calculated. Additionally, a cushion block compression and offset testing platform was set up for localized experiments to analyze the impact of cushion blocks on wire performance.

3.1. Calculation of Winding Electromagnetic Forces

The magnetic field is the bridge between the primary and secondary windings for energy transfer. Transformer internal and external windings are usually wound according to a certain type. Assuming that the number of turns of the primary side winding is N, it can be approximated as N coaxial conducting loops arranged in sequence [28]. The resulting spatial magnetic field exhibits axial symmetry. Therefore, a cylindrical coordinate system is established with the center axis of the conducting loops as the z-axis, assuming that the direction of the current is in the same direction as the line element dl.

According to Biot–Savart Law, for a conducting ring located at the point $(0, z_1)$ with radius r_1, the magnetic field dB generated at any point $A(r, z)$ in the surrounding space due to the line element dl is given by the following [29]:

$$\mathrm{d}B = \frac{\mu_0 I d\mathbf{l} \times \mathbf{r}(A_1, A)}{4\pi |\mathbf{r}(A_1, A)|^3} \tag{15}$$

where μ represents the permeability of free space, $\mathbf{r}(A_1, A)$ denotes the vector from point A_1 on the conducting loop to any point A in space, and I is the current flowing through the loop.

$\mathbf{r}(A_1, A)$ can be expressed as follows:

$$\mathbf{r}(A_1, A) = \mathbf{r}(A) - \mathbf{r}(A_1) = (r - r_1 \cos\theta, -r_1 \sin\theta, z - z_1) \tag{16}$$

The line element dl can be expressed as follows:

$$\mathrm{d}\mathbf{l} = (-r_1 \sin\theta d\theta, r_1 \cos\theta d\theta, 0) \tag{17}$$

Substituting (16) and (17) into (15) for integration calculation gives the following:

$$B = \frac{\mu_0 I}{4\pi} \int_0^{2\pi} \left[\frac{r_1 \cos\theta(z - z_1)i + r_1 \sin\theta(z - z_1)j}{[r^2 - 2r_1 r \cos\theta + r_1^2 + (z - z_1)^2]^{\frac{3}{2}}} + \frac{(r_1^2 - r_1 r \cos\theta)k}{[r^2 - 2r_1 r \cos\theta + r_1^2 + (z - z_1)^2]^{\frac{3}{2}}} \right] \mathrm{d}\theta \tag{18}$$

For ease of analysis, the magnetic flux density is typically divided into axial and radial components, which are represented as follows [30]:

$$B_z = \frac{\mu_0 I}{2\pi} \int_0^{\pi} \frac{(r_1^2 - r_1 r \cos\theta)}{[r^2 - 2r_1 r \cos\theta + r_1^2 + (z - z_1)^2]^{\frac{3}{2}}} \mathrm{d}\theta \tag{19}$$

$$B_r = \frac{\mu_0 I}{2\pi} \int_0^{\pi} \frac{(z - z_1)}{[r^2 - 2r_1 r \cos\theta + r_1^2 + (z - z_1)^2]^{\frac{3}{2}}} \mathrm{d}\theta \tag{20}$$

Using the Lorenz force calculation method, the radial and axial short-circuit electromagnetic forces experienced by the winding during transformer short-circuit conditions can be calculated using the following equations:

$$F_r = \int_V \mathbf{J} \times \mathbf{B}_z \, dv \tag{21}$$

$$F_z = \int_V \mathbf{J} \times \mathbf{B}_r \, dv \tag{22}$$

where $\mathbf{J}$ denotes the winding's short-circuit current density; $\mathbf{B}_z$ and $\mathbf{B}_r$ denote the axial and radial magnetic flux densities of the winding, respectively; and F_r and F_z denote the magnitudes of the radial and axial short-circuit electromagnetic forces on the winding.

3.2. Simulation Analysis of Winding Unbalanced Force after Short Circuit

Based on the SFSZ7-31500/110 prototype transformer (Liaoning Hengyi electric power Equipment Manufacturing Co., LTD., Shenyang, China), an electromagnetic force finite element simulation model was established for electromagnetic force calculation [31], as depicted in Figure 3. The main geometric parameters of the transformer are shown in Table 1. The material parameters of windings and the cushion blocks are detailed in Table 2.
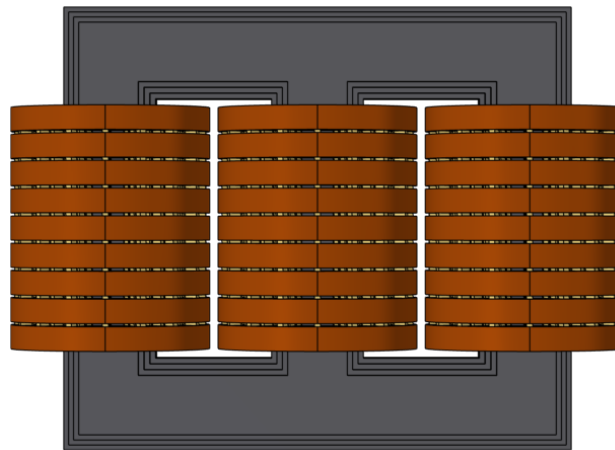

Figure 3. Schematic diagram of finite element simulation model of transformer electromagnetic force.

Table 1. Main geometric parameters of the transformer.

Parameter	Value
Low-Voltage Winding Inner Diameter/mm	331
Low-Voltage Winding Outer Diameter/mm	396
Medium-Voltage Winding Inner Diameter/mm	435
Medium-Voltage Winding Outer Diameter/mm	500
High-Voltage Winding Inner Diameter/mm	547
High-Voltage Winding Outer Diameter/mm	640.5
Low-Voltage Winding Turns	107
Medium-Voltage Winding Turns	226
High-Voltage Winding Turns	647
Window Height/mm	1670
Core Diameter/mm	600

Table 2. Material parameters for winding and cushion block.

Physical Quantity	Young's Modulus [MPa]	Density [g/cm^3]	Poisson's Ratio
Winding	124,000	8.96	0.325
Cushion Block	7600	1.3	0.34

The radial magnetic induction intensity in the middle of the transformer winding is nearly zero 0.01 s after a short circuit. The maximum axial electromagnetic force is generated at the ends, and its direction is opposite. Excessive electromagnetic force can lead to axial instability in the winding [32]. To study the structural stability at the location of maximum stress in the winding, the topmost layer of the medium-voltage winding was selected to observe the axial force distribution, as shown in Figure 4. It is evident that there is a localized unbalanced stress on the winding. The maximum axial electromagnetic forces are generated at the upper and lower ends of the winding, and they are in opposite directions; the maximum value is 1.88×10^9 N/m^3 and it is in the negative direction.
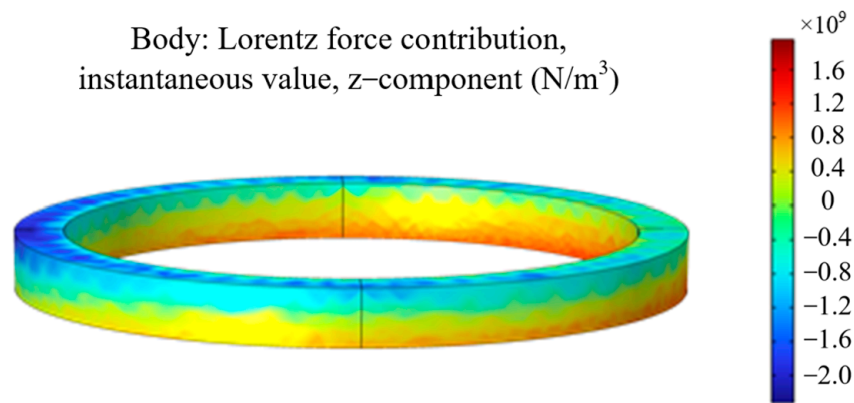

Figure 4. Axial force distribution at different positions of the same winding line.

The copper material used in transformer windings is a typical elastic–plastic material, with the stress–strain relationship described by the yield strength [33]. Cushion blocks are typically composed of nonlinear materials such as wood fiber or epoxy resin. According to the previous research results [34], it is generally believed that, when the value of the stress is less than 103 MPa, the stress–strain relationship of the insulation pad can be approximated as follows [35]:

$$\sigma = a\varepsilon + b\varepsilon^3 \tag{23}$$

where the linear constant a = 105.8 MPa and the hardening coefficient b = 1750 MPa.

The defining equation of the elastic modulus is shown in (24), from which the relationship between the elastic modulus E and the strain value is obtained as (25). And the elastic modulus–strain relationship of the cushion blocks is plotted, as shown in Figure 5.

$$E = \frac{d\sigma}{d\varepsilon} \tag{24}$$
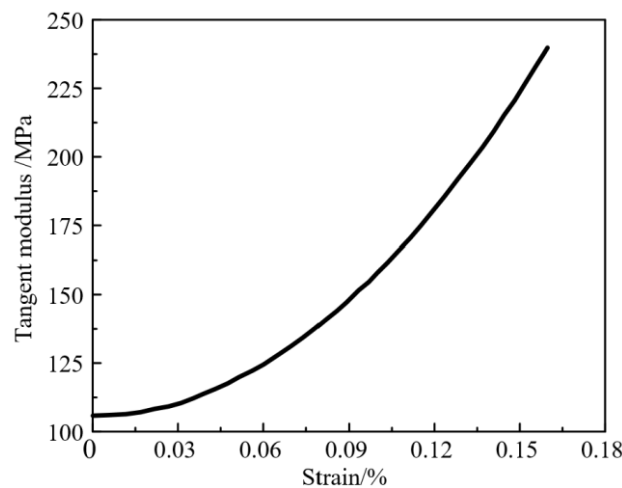
$$E = 105.8 + 5250\varepsilon^2 \tag{25}$$

Figure 5. Cushion block tangent modulus–strain curve.

From Figure 4, the Lorentz force density and the axial height can be used to calculate the equivalent surface stress distribution of insulating cushion blocks. Based on the axial force distribution at different positions, the maximum difference in stress between adjacent cushion blocks on the circumference can be determined. Using Equation (23) and the stress–strain relationship for cushion blocks, the corresponding maximum unbalanced strain range can be calculated. Finally, the maximum cushion block unbalanced height is found to be 5.3 mm. The specific calculation process is shown in Figure 6. This value can serve as the basis for setting cushion block unbalanced heights in subsequent experiments and simulations. It allows for the study of the impact of cushion-block-compression-induced unbalance in the axial strength of windings.
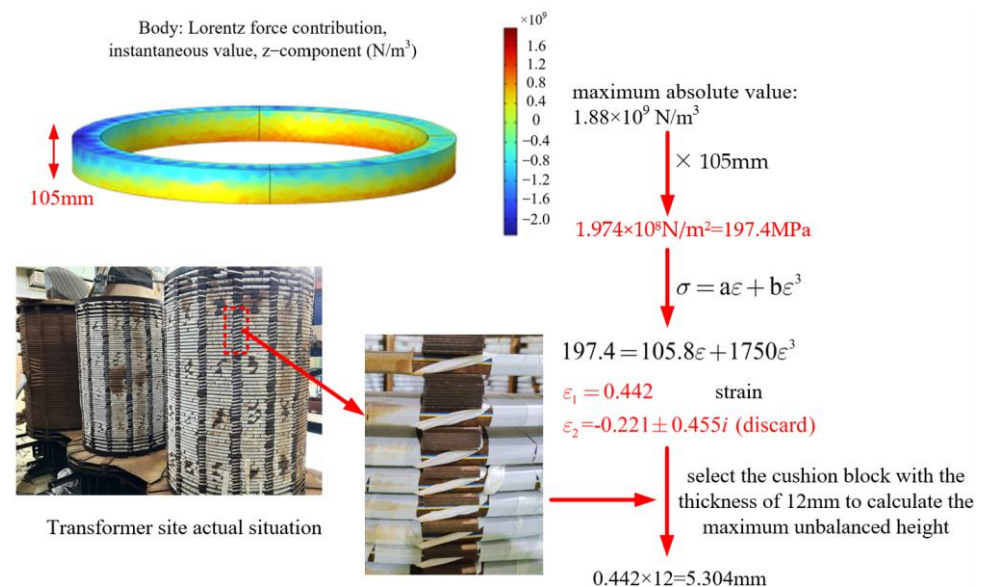

Figure 6. Maximum unbalanced height calculation illustration.

3.3. Analysis of Three-Point Bending Test

In this section, an experiment platform for cushion block compression and offset was set up. Insulating cushion blocks measuring 77 mm in length, 39 mm in width, and 2 mm in thickness were used. Rectangular copper wires were cut into several small segments of the required length and flattened using pliers. These segments were then tightly bound together with adhesive tape in groups of five, and two sets of insulating cushion blocks were used as endpoints to form the main structure for the three-point bending test. The wire samples were secured at both ends with fixtures. The wire bending tests were conducted

using an electronic universal testing machine with the model number ETM504D. During the testing process, a clamp moving speed of 2 mm/min was maintained, and a continuous bending force was applied to the rectangular specimens, with the force–deflection curve being automatically recorded. The test procedure is illustrated in Figure 7.
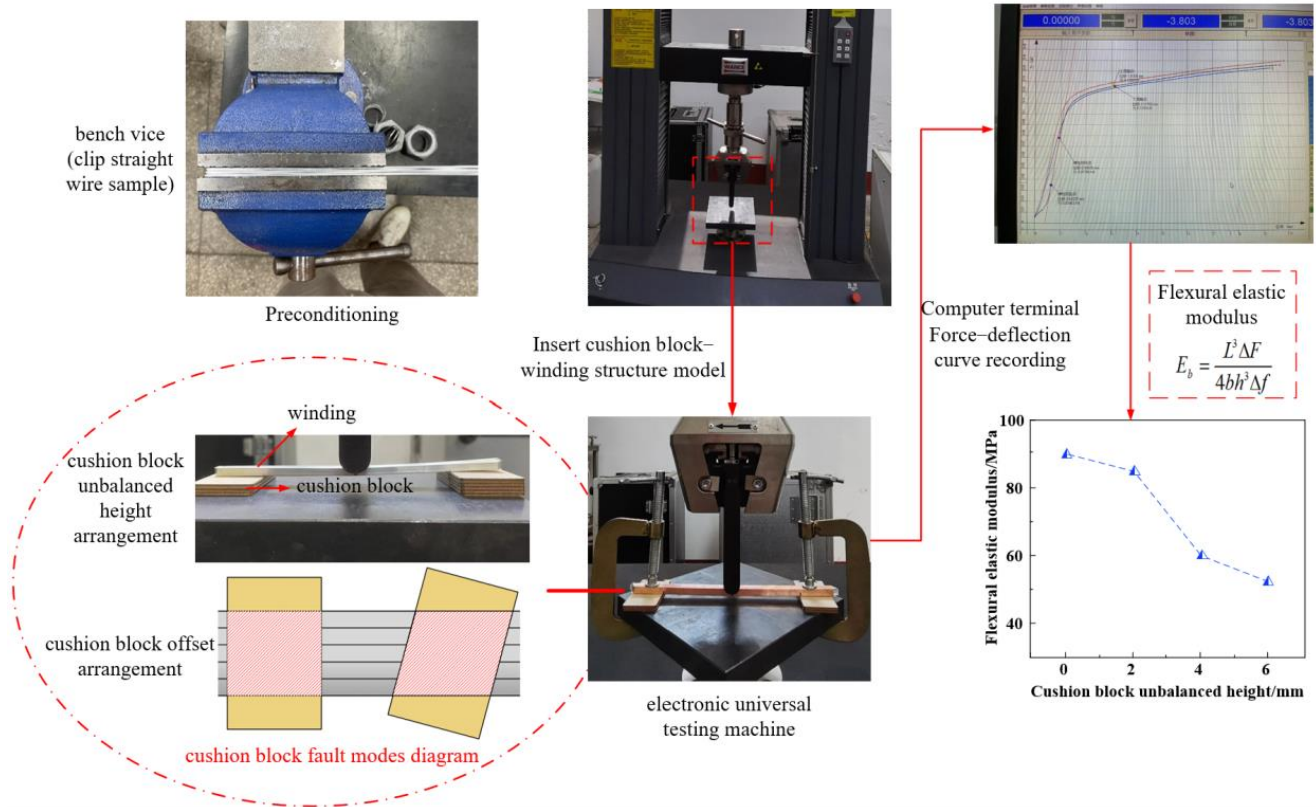

Figure 7. Flow chart of cushion block compression offset test.

Under the influence of axial forces, the winding can undergo compressive deformation, leading to a reduction in axial height, structural relaxation, and a lack of axial compressive force within the winding. Because the insulating cushion blocks between windings are continuously subjected to axial compression forces, the unbalanced heights of some cushion blocks may vary. Additionally, under the action of axial forces, the internal fibers of certain cushion blocks will gradually break, resulting in plastic deformation [36] and further compression. This leads to an increase in the unbalanced heights of adjacent cushion blocks and causes the support structure to become lax.

When studying the impact of cushion block unbalanced heights on the mechanical properties of the wire, different numbers of cushion blocks (ranging from 2 to 5) were stacked to achieve varying unbalanced heights between adjacent cushion blocks. Specifically, the unbalanced heights of the cushion blocks at both ends were set at 0, 2, 4, and 6 mm, respectively. To investigate the effect of cushion block offset, six sets of experiments were conducted, involving single-end cushion block offset, two-end cushion block offset in the same direction, and two-end cushion block offset in opposite directions of 30° and 45°. Taking 30° as an example, three different offset positions for the cushion blocks are explained, as shown in Figure 8. The simulation results yield axial bending stress cloud maps for the winding. A continuous bending force was applied to the center point of the rectangular specimens, and their force–deflection curves were recorded, respectively.
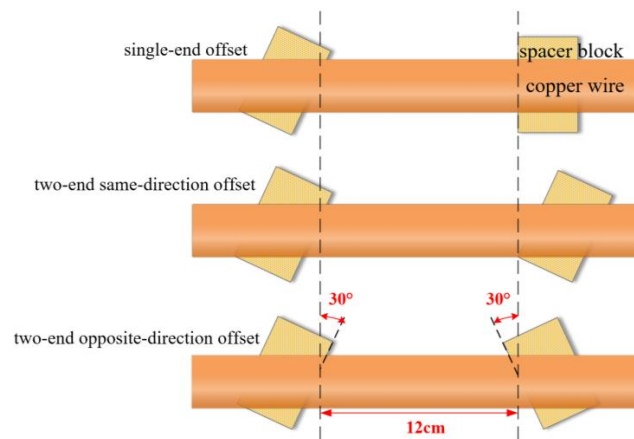
Figure 8. Example of cushion block offset structures.

For the purpose of comparative analysis, the bending elastic modulus of the wire under the three-point bending test was calculated in accordance with YB/T 5349-2006 [37]. Figure 9 illustrates the three-point bending test, where the wire is part of a beam-like structure composed of cushion blocks. The wire is placed transversely between the supports of the two end cushion blocks with a span length *L*. In the middle of the wire, a concentrated force F acts downward, causing bending, and f represents the deflection in millimeters.
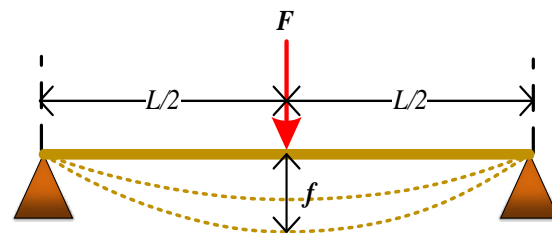

Figure 9. Schematic diagram of three-point bending test.

With reference to YB/T 5349 2006, the force–deflection curve, as shown in Figure 10, was measured by the universal testing machine. On the force–deflection curve, starting from the intersection point O of the elastic straight-line segment with the deflection axis, a segment $\overline{OC}$ corresponding to non-proportional bending strain is extracted and calculated according to Equation (26):

$$\overline{OC} = \frac{nL^2}{6h} \tag{26}$$

where *n* denotes the deflection magnification, *L* denotes the span of the wire, *h* denotes the height of the wire, and ε_{pd} denotes the specified non-proportional bending strain.
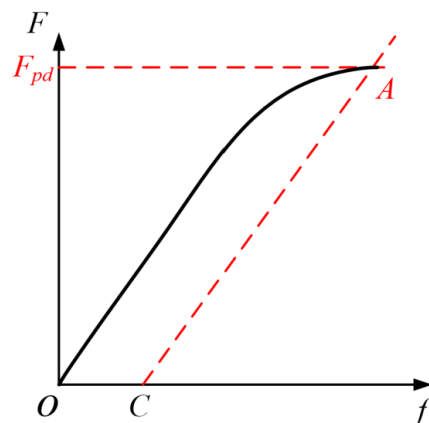

Figure 10. Graphical determination of non-proportional bending stress.

Through point C, make CA parallel to the elastic straight line segment to intersect the curve at point A. The force corresponding to point A is the measured prescribed non-proportional bending force F_{pd}. b is the width of the wire, and the prescribed non-proportional bending stress σ_{pd} of the wire can be calculated from Equation (27).

$$\sigma_{pd} = \frac{3F_{pd}L}{2bh^2} \tag{27}$$

Apply a pre-bending force of less than 10% $\sigma_{pd0.01}$ to the wire and record the force and deflection at the midpoint of the span. Then, continue loading the applied force until it reaches 50% $\sigma_{pd0.01}$. Record the incremental bending force and deflection at this point. Finally, calculate the bending modulus of elasticity using Equation (28).

$$E_b = \frac{L^3 \Delta F}{4bh^3 \Delta f} \tag{28}$$

where ΔF denotes the bending force increment and Δf denotes the deflection increment.

Firstly, the effect of unbalanced height of cushion blocks is studied and unbalanced support structures are set up at both ends of the wire. Set up the wire with two, three, four, and five pieces of cushion blocks support at one end and five pieces of cushion blocks support at the other end with a span of 17 cm. A total of five tests were carried out in each case and the average of the measurements was taken.

As can be seen from the Figure 11, there is a clear correlation between the cushion block unbalanced height and the force–deflection curve. With the increase in the unbalanced height of the neighboring cushion blocks, the bending force of the wire samples all show a decreasing trend, but the magnitude is not large. When the deflection reaches 5.8 mm, the bending force is 1.14 kN, 1.19 kN, 1.25 kN, and 1.25 kN in order when the cushion block unbalanced heights at both ends of the samples are 6, 4, 2, and 0 mm.
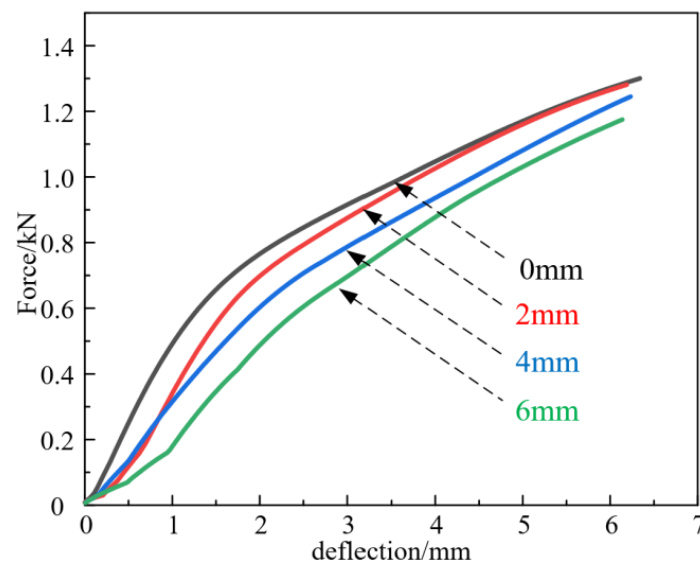

Figure 11. Force–deflection curves under different unbalanced heights of cushion blocks.

Similarly, the force–deflection curves of wires under different cushion block offsets are recorded, as shown in Figure 12, and, finally, the bending modulus of elasticity of multiple parallel-wound wires under different cushion block unbalanced heights and different cushion block offsets are obtained by the bending modulus of elasticity calculation method of Equation (26); the results are shown in Tables 3 and 4.
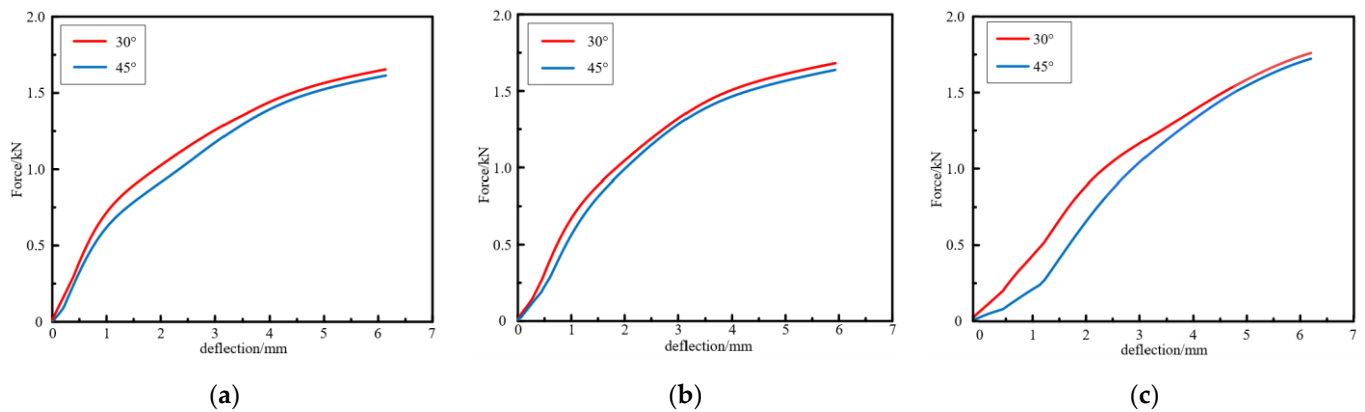
(a)   (b)   (c)

Figure 12. Force–deflection curves under different offsets of cushion block. (**a**) Single-end offset. (**b**) Two-end same-direction offset. (**c**) Two-end opposite-direction offset.

Table 3. Flexural modulus of elasticity with different cushion block unbalanced heights.

Cushion Block Unbalanced Height [mm]	Flexural Modulus of Elasticity [MPa]
6	52.22
4	59.86
2	84.86
0	89.97

Table 4. Flexural elastic modulus for different cushion block offsets.

Offset Angle	Single-End Offset Bending Elastic Modulus [MPa]	Two-End Same-Direction Offset Bending Elastic Modulus [MPa]	Two-End Opposite-Direction Offset Bending Elastic Modulus [MPa]
30°	53.76	46.29	33.64
45°	52.85	40.80	18.64

Based on the data in the table, it can be observed that, as the height of adjacent cushion block unbalances increases, the bending elastic modulus of the wire decreases. When the cushion block unbalanced height increases from 0 mm to 2 mm or from 4 mm to 6 mm, the average decrease in the bending elastic modulus of the samples is approximately 6.37 MPa. When the cushion block unbalanced height increases from 2 mm to 4 mm, the change in the bending elastic modulus of the samples is 25.00 MPa, representing a decrease of 29.46%. Under the same offset angle, the wire's bending elastic modulus is lowest for the cushion block's crosswise offset structure, indicating the poorest mechanical performance. The cushion block's same-direction offset structure follows. For both 30° and 45° offset angles, the bending elastic modulus of the wire under these three offset structures decreases as the offset angle increases, indicating deteriorating mechanical performance. When the cushion block offset angle is 45°, the bending elastic modulus of the wire decreases by 54.7% and 79.3% for same-direction and crosswise offsets, respectively. This may be attributed to the reduced contact area between the cushion blocks and the winding due to cushion block offset, leading to weakened bending resistance.

4. Impact Analysis of Cushion Blocks on Winding Axial Strength

In order to study the reliability of the test, a three-cake toroidal model of the transformer in finite element simulation software is built in this section, calculates and analyzes the maximum axial bending stresses of the windings with different cushion block unbal-

anced heights and different cushion block offsets, and verifies the consistency of the change trend.

4.1. Transformer Three-Cake Toroidal Model Construction

To investigate the specific impact of cushion blocks on the axial strength of transformer windings, this section uses finite element simulation software to create a three-layer toroidal model of the transformer [38]. The model includes medium-voltage windings and cushion blocks, as shown in Figure 13. In the model, each coil has a thickness of 12 mm, and each set of insulating cushion blocks is 77 mm in length, 39 mm in width, and 10 mm in thickness. Sixteen sets are uniformly installed between the transformer coils. The inner diameter of the medium-voltage winding is 435 mm, and the outer diameter is 500 mm. The material parameters of the windings and cushion blocks are consistent with those selected in Section 3.2.
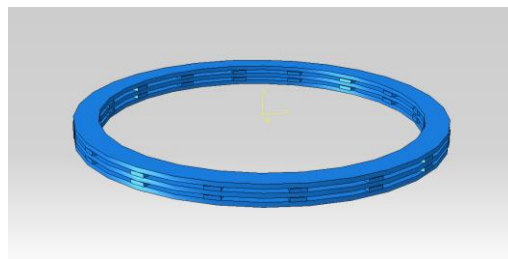

Figure 13. Model of the winding and cushion block support structure.

4.2. Impact of Cushion Block Unbalanced Height on Winding Axial Strength

To investigate the impact of the cushion block unbalanced height on the axial strength of the transformer winding, a control group with one layer of 16 sets of cushion blocks, each with a total thickness of 10 mm, is set as the baseline. A maximum compression of 6 mm is set for the simulation analysis of cushion block height unbalances. One set of cushion blocks in the bottom layer was selected, and the total thickness of the cushion blocks is separately set to 8 mm, 6 mm, and 4 mm, corresponding to unbalanced heights with adjacent cushion blocks of 2 mm, 4 mm, and 6 mm. The resulting axial bending stress distribution maps are shown in Figure 14.
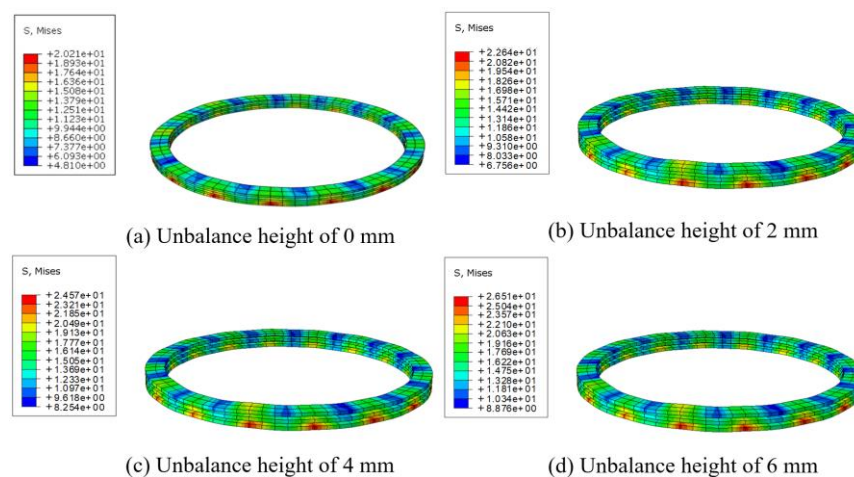

(a) Unbalance height of 0 mm

(b) Unbalance height of 2 mm

(c) Unbalance height of 4 mm

(d) Unbalance height of 6 mm

Figure 14. Winding axial bending stress cloud for different cushion block unbalanced heights.

It can be seen that, in the control group, when the cushion block unbalanced height is 0 mm, the maximum axial bending stress in the winding is 20.21 MPa. With a cushion block unbalanced height of 2 mm, 4 mm, and 6 mm, the maximum axial bending stress in the winding increases to 22.64 MPa, 24.57 MPa, and 26.51 MPa, respectively. The results

are plotted in the line chart shown in Figure 15. The test results under different unbalance heights are shown in Table 5.
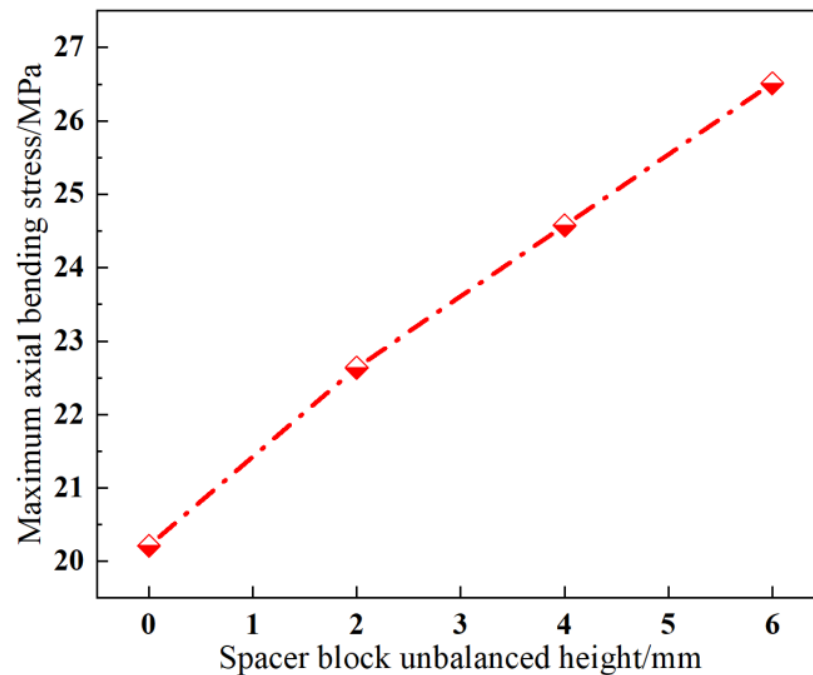

Figure 15. Maximum axial bending stress in the winding with different cushion block unbalanced heights.

Table 5. Comparison of test results under different unbalanced heights.

Cushion Block Unbalanced Height [mm]	Flexural Modulus of Elasticity [MPa]	Maximum Axial Bending Stress [MPa]
0	89.97	20.21
2	84.86	22.64
4	59.89	24.57
6	52.22	26.51

It can be seen from the table that, with the increase in the unbalanced height of the cushion blocks, the flexural elastic modulus of the winding decreases, which means that the winding is more prone to deformation when subjected to the same stress, and the short-circuit resistance decreases. The increase in the maximum axial bending stress on the winding, that is, the stress on the winding, will increase, and the deformation risk of the winding will also increase. The results obtained from the test and simulation are consistent, which verifies the feasibility of the structural part test.

4.3. Impact of Cushion Block Offset on Winding Axial Strength

To investigate the influence of cushion block offset on the axial strength of the winding, three cushion block offset structures are set up, including a single-end offset, two-end same-direction offset, and two-end anisotropic offset. Four offset angles are considered, including 15°, 30°, 45°, and 60°. Three cases with offset angles of 30°, 45°, and 60° are presented in Figure 16. The line chart depicting the maximum axial bending stress under conditions is shown in Figure 17.
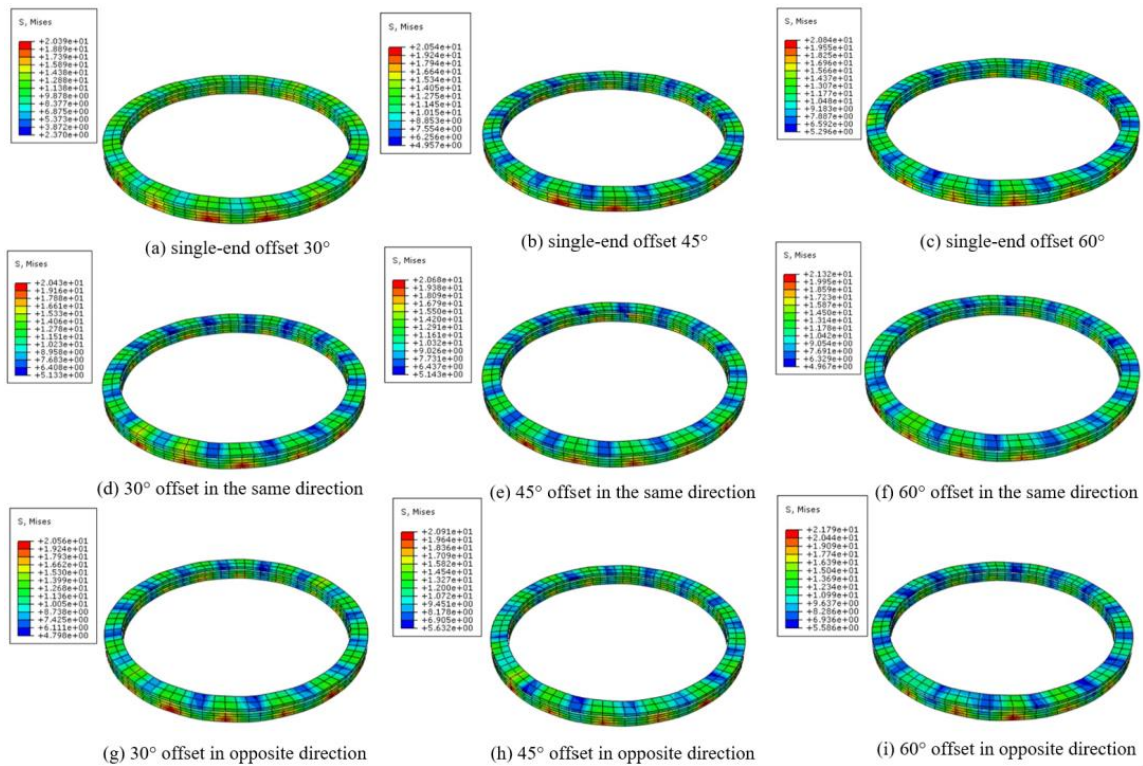
Figure 16. Winding axial bending stress cloud for different cushion block offsets.
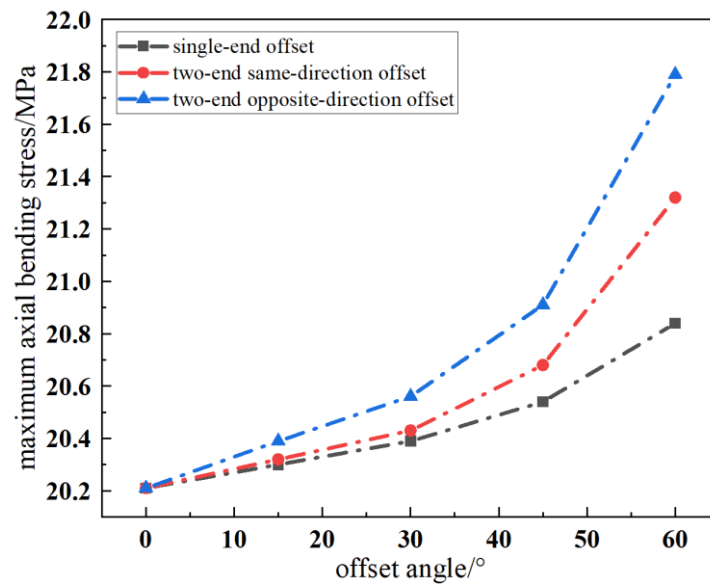

Figure 17. Maximum winding axial bending stress in the winding for different cushion block offsets.

It can be observed that, for windings with different cushion block offset structures, as the cushion block offset angle increases, the trend in the change of the maximum axial bending stress in the windings is the same, showing an increasing pattern. Moreover, as the offset angle increases to a certain degree, the magnitude of the increase in the maximum axial bending stress gradually rises, exacerbating the impact of the offset angle on winding strength.

Different offset structures have varying effects on winding strength. Under the same cushion block offset angle, windings with cushion blocks deviating in opposite directions consistently exhibit the highest maximum axial bending stress, while windings with single-end offset structures consistently have the lowest maximum axial bending stress. In the

range of offset angles from 0° to 15°, the impact of different cushion block offset structures on winding axial strength is relatively small. However, as the offset angle increases, the magnitude of the increase in maximum axial bending stress for each structure also increases. Among these structures, those with opposite-direction offset show the most significant increase, leading to the greatest reduction in winding axial strength. The overall simulation trends align well with the experimental results, validating the effectiveness of the experiments.

5. Conclusions

During the short-circuit process of transformers, the axial unbalanced force leads to cushion block compression and offset, causing axial instability in the winding. This paper establishes a test platform for cushion block compression and offset, investigates the effects of cushion block unbalanced height and cushion block offset on the axial strength of the windings, and validates the results in combination with finite element simulation outcomes. The following conclusions are drawn:

1.　The axial strength of the winding-cushion block composite structure is affected by the cushion block height unbalanced Δl and the cushion block offset angle θ. Cushion block compression faults can affect the unbalanced height Δl, while cushion block offset faults directly affect the offset angle θ. Cushion block compression and offset faults lead to an increase in the axial bending stress of the winding-cushion block structure, posing a more severe challenge to the axial strength of the winding.
2.　A greater cushion block unbalanced height results in higher bending elastic modulus and lower axial strength in the windings. When the unbalanced height is 2 mm, 4 mm, and 6 mm, the maximum axial bending stress in the windings increases by 12.02%, 21.57%, and 31.17%, respectively. The impact of increasing cushion block unbalanced height on winding strength reduction is almost linear.
3.　Under the same offset angle, the winding's bending elastic modulus is lowest for the cushion block opposite-direction offset structure, indicating the poorest mechanical performance. The cushion block's same-direction offset structure follows. For the axial bending stress in an opposite-direction offset structure, when the offset angle is 30°, 45°, and 60°, the maximum axial bending stress increases by 1.73%, 3.46%, and 7.82%, respectively, and the degree of reduction in the axial winding strength progressively intensifies.

References

1.　Bouderbala, R.; Bentarzi, H. Differential relay reliability enhancement using fourth harmonic for a large power transformer. *Int. J. Syst. Assur. Eng. Manag.* **2017**, *8*, 592–598. [CrossRef]
2.　Bakshi, A.; Kulkarni, S.V. Analysis of buckling strength of inner windings in transformers under radial short-circuit forces. *IEEE Trans. Power Deliv.* **2014**, *29*, 241–245. [CrossRef]

3. Zhang, J. Analysis of Leakage Field and Short-Circuit Electric Force in Transformer Windings. Master's thesis, Shenyang University of Technology, Shenyang, China, 2019.

4. Huang, Q. Study on Short Circuit Stability of Transformer Based on Finite Element Simulation. Master's thesis, Huazhong University of Science & Technology, Wuhan, China, 2017.

5. Dawood, K.; Komurgoz, G.; Isik, F. Computation of the axial and radial forces in the windings of the power transformer. In Proceedings of the 2019 4th International Conference on Power Electronics and their Applications (ICPEA), Elazig, Turkey, 25–27 September 2019; pp. 1–6.

6. Yadav, S.; Mehta, R.K. FEM based study of short circuit forces on power transformer windings. In Proceedings of the 2019 3rd International Conference on Recent Developments in Control, Automation & Power Engineering (RDCAPE), Noida, India, 10–11 October 2019; pp. 540–544.

7. Linda, L.; Zhengxu, L.; Shiyuan, S. Research Review on Short-Circuit Cumulative Effect of Power Transformer. *Transformer* **2017**, *54*, 24–31.

8. Fan, Z.; Xiuguang, L.; Xiaoyu, Z. Assessment of the Withstand Ability to Short Circuit of Inner Windings in Power Transformers Considering the Degree of Thermal Aging. *Proc. CSEE* **2022**, *42*, 3836–3846.

9. Bo, Z.; Yan, L. Radial Stability of Large Transformer Windings under Multiple Inrush Conditions. *Trans. China Electrotech. Soc.* **2017**, *32*, 71–76.

10. Steel, R.B.; Johnson, W.M.; Narbus, J.J.; Patel, M.R.; Nelson, R.A. *Dynamic Measurements in Power Transformers under Short-Circuit Conditions*; CIGRE: Paris, France, 1972; pp. 1253–1258.

11. Andersen, O.W. Transformer Leakage Flux Program Based on the FEM. *IEEE Trans. Power Appar. Syst.* **1973**, *92*, 682–689. [CrossRef]

12. Kawanishi, K.; Suzuki, T.; Kosakaetal, M. Axial behavior of transformer windings on short-cireuit(Part2). *IEEE Trans. Power Appar. Syst.* **1999**, *13*, 418–423.

13. Zhao, Z.; Li, G.; Li, J.; Zhang, S.; Liu, Y.; Gao, F. Analyzing the Short-circuit Withstanding Ability of Large Power Transformer Based the FEM Method. *High Volt. Eng.* **2014**, *40*, 3214–3220.

14. Bo, Z.; Yan, L.; Ning, Y. Calculation of Short-Circuit Strength of Windings in Power Transformer based on Strong Coupling. *Transformer* **2015**, *52*, 6–9.

15. Dexu, Z.; Yigu, Q.; Guochao, Q. Axial Force Distribution Characteristics and Test Analysis of Transformer under Short-Circuit Condition. *Transformer* **2020**, *57*, 24–28.

16. Wang, Y.; Zhou, G.; Zeng, C.; Zhang, W.; Ren, Y.; Ke, Y.; Chu, H.; Suo, C. Research on online detection method of transformer winding deformation based on VFTO. *Sensors* **2021**, *21*, 7386. [CrossRef] [PubMed]

17. Fan, Z.; Cheng, M.; Xiuguang, L. Dynamic Assessment of Windings' Axial Mechanical Strength in Power Transformers Considering the Vibration Response. *Proc. CSEE* **2022**, *43*, 1–11. [CrossRef]

18. Jichao, C. Simulation Study on Strength of Winding and Supporting Structure of Power Transformer under Short Circuit Condition. Master's Thesis, Shenyang University of Technology, Shenyang, China, 2022.

19. Oria, C.; Carrascal, I.; Ferreño, D.; Méndez, C.; Ortiz, A. Experimental dataset on the compressive mechanical properties of high-density pressboard used in power transformers spacers. *Data Brief* **2023**, *50*, 109471. [CrossRef]

20. Oria, C.; Méndez, C.; Carrascal, I.; Ferreño, D.; Ortiz, A. Degradation of the compression strength of spacers made of high-density pressboard used in power transformers under the influence of thermal ageing. *Cellulose* **2023**, *30*, 6539–6558. [CrossRef]

21. Ou, Q.; Luo, L.; Li, Y.; Han, R.; Peng, Y. An Improved Radial Buckling Analysis Method and Test Investigation for Power Transformer under Short Circuit Impact. *IEEE Trans. Power Deliv.* **2023**, *38*, 2854–2863. [CrossRef]

22. Ou, Q.; Luo, L.; Li, Y.; Li, Y.; Xiang, J. Buckling Strength Investigation for Power Transformer Winding Under Short Circuit Impact Considering Manufacture and Operation. *IEEE Access* **2023**, *11*, 7850–7859. [CrossRef]

23. Kumar, I.; Bakshi, A. Effect of Flexibility of Axial Supporting Spacers on the Buckling Strength of Transformer Inner Winding. In Proceedings of the 2022 7th International Advanced Research Workshop on Transformers, Baiona, Spain, 23–26 October 2022; pp. 87–91.

24. Kaiqi, L. Study on Calibration Models and Evaluation Technology for Short Circuit Withstand Ability of Power Transformer. Master's Thesis, Nanjing University of Aeronautics and Astronautics, Nanjing, China, 2016.

25. Lei, Y.; Richang, X.; Qingyu, R. Effect Analysis of Winding Structure on Short-Circuit Force of Distribution Transformer. *Transformer* **2020**, *57*, 28–32.

26. Shenghan, S.; Xiaohua, L.; Fuyuan, C. Influence of Long-Term DC Magnetic Bias Operation on Cushion Offset and Anti-Short Circuit Ability of Transformer. *Transformer* **2021**, *58*, 24–29.

27. *GB/T 1094.5-2008*; Power Transformers-Part 5: Ability to Withstand Short Circuit. China National Standards: Beijing, China, 2008.

28. Wanchao, W. Research on Mechanical Strength and Stability of Transformer Windings under Multiple Short-circuit Conditions. Master's Thesis, Shenyang University of Technology, Shenyang, China, 2017.

29. Meng, T.; Li, Y.; Li, P.; Wang, X.; Hou, B.; Yu, Z. Research on distribution of winding leakage magnetic field of three-phase dry type transformer under short-circuit condition. *Energy Rep.* **2023**, *9*, 1108–1115. [CrossRef]

30. Wang, S.; Wang, S.; Zhang, N.; Yuan, D.; Qiu, H. Calculation and Analysis of Mechanical Characteristics of Transformer Windings Under Short-Circuit Condition. *IEEE Trans. Magn.* **2019**, *55*, 8401804. [CrossRef]

31. Li, Z.; Tan, Y.; Li, Y.; Yang, X.; Su, Z.; Liu, J.; Wang, S.; Wang, Y. Radial stability evaluation and cumulative test of transformer windingsunder short-circuit condition. *Electr. Power Syst. Res.* **2023**, *217*, 109112. [CrossRef]

32. Li, Z.; Hao, Z.; Yan, C.; Wang, K.; Dang, Y.; Xu, H.; Zhang, B. Axial stability analysis and simulation of power transformer windings. In Proceedings of the 2016 IEEE PES Asia-Pacific Power and Energy Engineering Conference (APPEEC), Xi'an, China, 25–28 October 2016; pp. 1665–1669.

33. Ren, F.; Ji, S.; Zhu, L. Experimental Research on Cumulative Deformation of Transformer Winding Induced by Short-Circuit Current Impacts. In Proceedings of the In 2019 21st International Symposium on High Voltage Engineering (ISH), Budapest, Hungary, 26–30 August 2019; pp. 625–634.

34. Zhou, H.; Hong, K.; Huang, H.; Zhou, J. Transformer winding fault detection by vibration analysis methods. *Appl. Acoust.* **2016**, *114*, 136–146. [CrossRef]

35. Wang, J.; Xing, Y.; Ma, X.; Zhao, Z.; Yang, L. Numerical Investigations for Vibration and Deformation of Power Transformer Windings under Short-Circuit Condition. *Energies* **2023**, *16*, 5318. [CrossRef]

36. Lin, X.; Liu, J.; Wang, F.; Ai, W.; Li, Z.; Chen, S. Magnetic-Structural Coupled Simulation of Power Transformer Winding Cumulative Effect. In Proceedings of the 2022 IEEE 5th International Electrical and Energy Conference (CIEEC), Nangjing, China, 27–29 May 2022; pp. 2860–2865.

37. *YB/T 5349-2006*; Test Methods for Mechanical Properties of Metal Bending. China National Standards: Beijing, China, 2006.

38. Luo, L.; Wen, X.; Luo, X.; Qin, W. Research on Axial Stability of Power Transformer Windings. In Proceedings of the 2022 4th International Conference on Smart Power & Internet Energy Systems (SPIES), Beijing, China, 9–12 December 2022; pp. 356–360.